JOURNAL OF MATERIALS SCIENCE 8 (1973) 807–829

Stress-strain characteristics and slip band formation in copper-base alloy crystals

F. D. ROSI
327 Dodds Lane, Princeton, New Jersey, USA

The plastic properties at room temperature of extended copper crystals alloyed with aluminium, germanium and silicon were examined as a function of crystal orientation, alloy concentration and nature of solute. A strong orientation dependence was observed on the gross shape of the shear stress/shear strain diagram in all of the alloy crystals examined. In those crystals exhibiting a well-defined two-stage hardening curve, the extent of shear associated with stage I and the shear hardening coefficients of stages I and II are significantly dependent on orientation, nature and concentration of solute. On the other hand, the shear stress defining the onset of stage II is constant and independent of crystal orientation. Variations in the gross shape of the shear stress/shear diagram and in the parameters defining the two-stage hardening curve are correlated with changes in slip line development. No evidence of Lüders band propagation, kink band development or twinning, was observed.

1. Introduction

The experimental work reported in this paper on the effect of solid solution alloying with aluminium, germanium and silicon on the plastic deformation of copper crystals was done about fifteen years ago. In spite of this time lapse, and the many significant papers published in the ensuing period in this particular area of crystal mechanics [1-15], the information still appears significant enough to bring to the attention of workers in this field.

The effect of alloying on the stress-strain characteristics of face-centred cubic crystals was first studied in a number of systems by both German and English investigators in the decade 1925-35 [16-24]. In general, this pioneering work showed that with increasing concentration of the alloying element in solid solution (1) the yield point becomes better defined by an abrupt occurrence of extensive elongation with little or no increase in stress (yield-point elongation phenomenon), (2) the critical resolved shear stress for the onset of plastic flow increases markedly though at a decreasing rate at high solute concentrations, and (3) the shear hardening of the initially latent conjugate slip system increases in relation to the active primary system, as evidenced by an "overshoot" of crystal orientation beyond the crystallographic symmetry position ($\langle 100\rangle - \langle 111\rangle$) associated with double slip. These earlier studies in the deformation of alloy crystals also showed a well-defined two-stage shear-hardening curve with the following characteristics: stage I immediately following the onset of plastic flow is associated with a low but often poorly defined rate of hardening, particularly at high alloy concentrations; stage II at higher extensions exhibits a much higher and approximately linear rate of shear hardening; the extent of shear associated with stage I increases markedly with increasing alloy content; and finally the rate of shear hardening in both stages I and II would appear to decrease with increasing solute concentration, particularly in the case of alpha-brass crystals [17, 20, 21]. All these observations have been confirmed in a wider variety of alloy systems by more recent investigators, whose work is summarized in the reviews by Clarebrough and Hargreaves [25] and Mitchell [26]. Several of these studies [2, 3, 12] also clearly established the existence of a yield-point phenomenon (double

yield-point) in a number of alloy systems at high solute concentrations.

In addition to the above stress-strain features, the early work of Sachs *et al* [20, 21] showed a marked tendency for slip markings to cluster with increasing deformation in alpha-brass crystals; and this clustering became more pronounced and common in alloys with large solute concentrations. Thus, alloying would appear to promote additional slip on the same crystallographic system in regions of the crystal where previous glide had occurred. The precise nature of this form of slip-band development was clearly shown by Treuting and Brick [27] and Maddin *et al* [28], and more recently Wilsdorf *et al* [29, 30], using electron microscopy techniques.

It is apparent from the foregoing that important generalizations can be drawn in connection with the effects of alloying on the manifestation and dynamics of glide in face-centred cubic metal crystals. However, it is difficult to draw definitive correlations between these generalizations. Much of the previous work did not take into account the effect of crystal orientation, which was later shown to have a considerable effect on the gross shape of the shear stress/shear strain diagram in pure metal crystals [31-33]. In addition, reliable conclusions based on a comparison of the more recent work of different investigators are made difficult by the variations in the size and surface preparation of the crystals, which have also been found recently to have a pronounced effect on the stress-strain curve [33, 34-37]. For these reasons, the present work was undertaken to re-examine a number of solid solution alloying effects in several dilute, binary copper-base systems at room temperature. Particular attention was directed toward examining and then eliminating the orientation effect, and standardization of crystal size and surface treatment. Hence, this effort represents a logical extension of a previous work on the orientation effect in face-centred cubic metal crystals [33].

2. Experimental procedure

The copper-base alloy system investigated in the present work were Cu-Al, Cu-Ge and Cu-Si. These systems exhibit reasonable amounts of solid solubility at room temperature, and the solute atoms have similar univalent ionic radii (Al-0.72, Ge-0.76 and Si-0.65Å) as compared with Cu (0.96Å) and also electronegativity values (Al-1.5, Ge-1.7 and Si-1.8) [38]. The alloys were made with OFHC copper and with solutes of highest attainable purity; and the solute concentrations selected for study were well within the solid solubility limits at room temperature. The vertical Bridgman method of gradual solidification from the melt [39] was used to produce single crystal specimens, 10 mm diameter and 13 cm long. The melting and solidification were done in graphite crucibles under a vacuum of 10^{-5} Torr, and with a crucible lowering rate of 6 mm h^{-1}. After deformation, each crystal was analysed chemically along it gauge length, and the variation in composition was never found to exceed 0.05% of the mean solute content. This small variation in composition is probably due to the small temperature difference between the liquidus and solidus curves in these dilute alloys. In cases where it was desirable to have crystals of identical orientation, the crystals were grown from a common seed; an example of three crystals grown from such a seed is shown in Fig. 1.

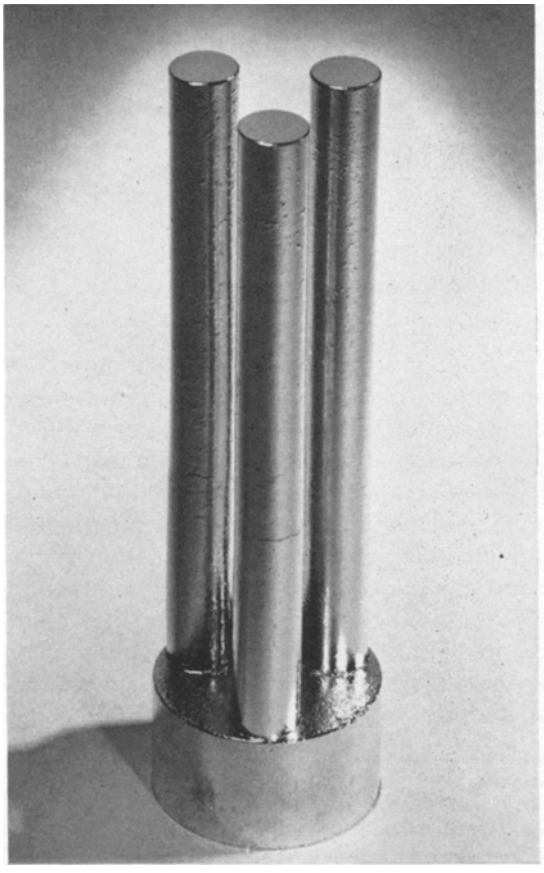

Figure 1 Three Cu-Al crystals of identical orientation and alloy composition grown from a common seed.

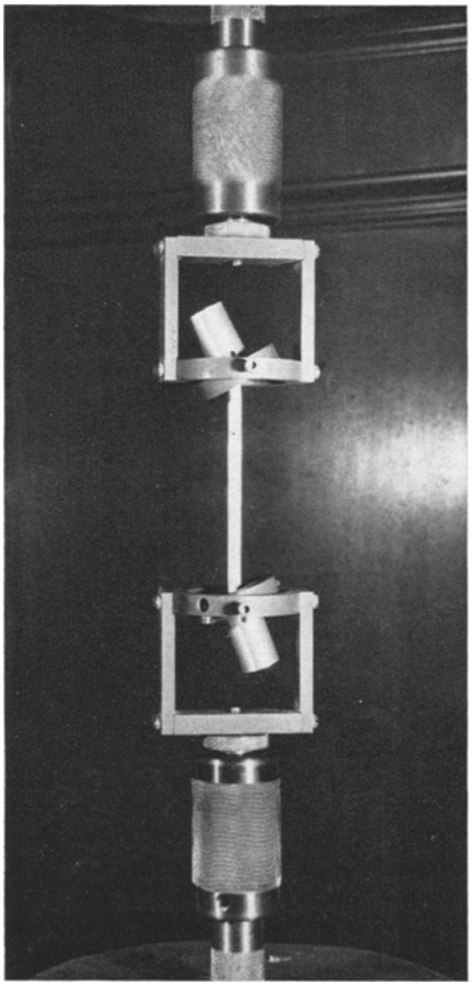

Figure 2 Copper single crystal extended in gimbal-grip arrangement in effort to avoid inhomogeneities of deformation associated with use of fixed grips.

The back-reflection Laue method was used for determining crystal orientation. In the specimens with high alloy content, the Laue photograms occasionally showed double diffraction spots indicative of the lineage type of structural imperfection discussed in detail by Buerger [40].

To obtain a 7.5 dm gauge length of uniform diameter and a surface suitable for optical microscopy, the as-cast crystals were coated at their ends with Duco cement, etched with constant agitation in a 30% solution of nitric acid, and then electrolytically polished. The polishing was done in a 2:1 solution of methyl alcohol and concentrated nitric acid at a current density of 15 to 20 A cm^{-2} for 10 to 15 min. All crystals were extended in the as-polished condition in air at room temperature.

Depending upon the nature of the required stress-strain data, either of two methods of tensile testing was used. The first of these involved equipment which would yield data pertinent to the evaluation of the critical resolved shear stress for the onset of plastic flow at a constant stressing rate of 325 g min^{-1}, while the second was used primarily to obtain the gross shape of the stress-strain diagram up to 25% extension at a constant strain-rate of 0.003 min^{-1}. A detailed description of these methods of tensile testing is given in a previous paper [33]. In both methods, a rotatable grip arrangement [41] was used in an attempt to eliminate the inhomogeneity of deformation in tension associated with the use of fixed grips (the so-called "grip effect"). The photograph in Fig. 2 shows a Cu single crystal being deformed in this gimbal grip arrangement. The angular displacement of the gripped ends of the crystal in opposite directions gives striking evidence that the high degree of conformal bending associated with the conventionally rigid type of tensile testing is avoided here by the gimbal action at both ends of the crystal gauge length. This is further supported by experiments where Cu crystals were extended approximately 10% in a manner such that one end was kept rigid while the other was free to rotate in the gimbal-grip arrangement of Fig. 2. An examination of Laue spots showed much more distortion at the rigid end of the crystal, and on annealing at 700°C recrystallization occurred first in this same region. Moreover, on annealing at higher temperatures up to 850°C, the recrystallization progressed gradually along the crystal toward its centre; yet at the end which was gripped in the gimbal assembly, there was still no evidence of recrystallization.

To examine the effect of this more homogeneous method of tensile deformation on the stress-strain characteristics, single crystals of identical orientations were extended at room temperature with and without the gimbal arrangement in Fig. 2. In both cases the strain was measured along the central 5.1 cm of a 7.5 cm gauge length. Therefore, the portion of the crystal in the vicinity of the gripped ends may not be expected to contribute appreciably to the determination of the stress-strain curves, except perhaps at very large deformations. Indeed, results from these tests, which were conducted on both copper and copper-base alloy crystals, indicated that there is no significant difference in

the value of the critical resolved shear stress for onset of flow for the two methods of testing. Moreover, in those crystals where considerable strain-hardening occurs immediately following the onset of plastic flow, there is also very little difference in the nature of the strain-hardening curves as a result of the different methods of gripping the specimens. On the other hand, when the stress-strain diagram exhibits a pronounced two-stage hardening process as in the case of the Cu-8% Al crystal in Fig. 3, effects are observed.

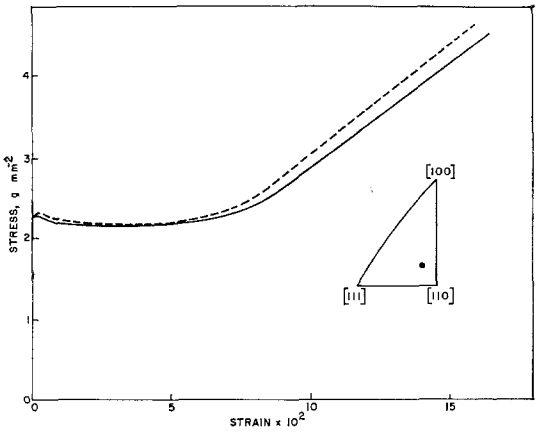

Figure 3 A comparison of stress-strain diagrams for Cu-8% Al crystals of identical orientation extended with (——) and without (- - - -) gimbal-grip arrangement.

The amount of strain associated with stage I is increased, and the linear strain-hardening in stage II decreases with the use of the gimbal-grip arrangement. However, these effects are not as striking as those discussed above in connection with the distortion of Laue spots and the preferential occurrence of recrystallization in the vicinity of the non-rotatable end of the crystal.

The formulae used in the evaluation of shear stress and shear strain, as in deriving the coefficient of shear hardening, are conveniently given by Schmid and Boas [42] in terms of the original orientation and the change in length of the crystal. In this connection, χ_0 and λ_0 represent the angles which the slip plane and slip direction originally make with the stress axis, respectively. For calculating the critical resolved shear stress for flow, the standard equation was used. The terminology used by Rosi and Mathewson [43] will be adopted in identifying the operative slip planes observed metallographically.

3. Experimental results and discussion

3.1. Critical shear stress

The determination of the critical resolved shear stress for the onset of plastic flow was made with alloy crystals whose original orientations adequately covered the standard stereographic triangle. The values of the critical shear stress were obtained from stress-strain curves by noting the value at which plastic flow set in at a rapid rate. As illustrated in a previous paper [33], the yield stress was taken as the extrapolated point which represents the intersection of the elastic range with the straight portion of the stress-strain curve, which occurs immediately after the onset of flow. In crystals where a distinct double yield point was observed, this arbitrary method of yield stress selection was not readily applicable; and in these cases, the yield stress was determined from the point of deviation from Hooke's law.

The validity of Schmid's critical resolved shear stress law could not be properly evaluated, because of the small differences in solute concentration between crystals of the same general alloy content. However, examination of the data for the more dilute Cu-Al alloy series revealed slightly higher values for orientations near ⟨100⟩. This same effect was observed in high-purity copper and silver [33, 44] and aluminium [32]. It is possible that the presumably higher values of S_0 near a ⟨100⟩, simply reflect the ill-defined nature of the yield point for this critical orientation as a result of the high rate of strain-hardening following the onset of plastic flow.

The critical shear stress data are summarized in the curves of Fig. 4, which also includes for comparison the data of Haasen and King [11] on Cu-Ge and Koppenaal and Fine [12] on Cu-Al. It may be seen that S_0 increases rapidy with increasing alloy content, and at an approximately linear rate for the more dilute (0 to 2.5 at.%) alloys in the Cu-Ge and Cu-Si systems. This latter dependence is supported by the studies of Linde *et al* [1] of a number of dilute alloy systems, including Cu-Ge and Cu-Si. It is also evident from Fig. 4 that the Group IV solute elements, silicon and germanium, are more effective in raising the critical shear stress than aluminium. For example, at a solute content of 4% the value of S_0 increases by a factor of approximately 9 for Cu-Al as against 13 for Cu-Ge. As in the earlier work of von Göler and Sachs [21] on Cu-Zn alloys, Sachs and Weerts

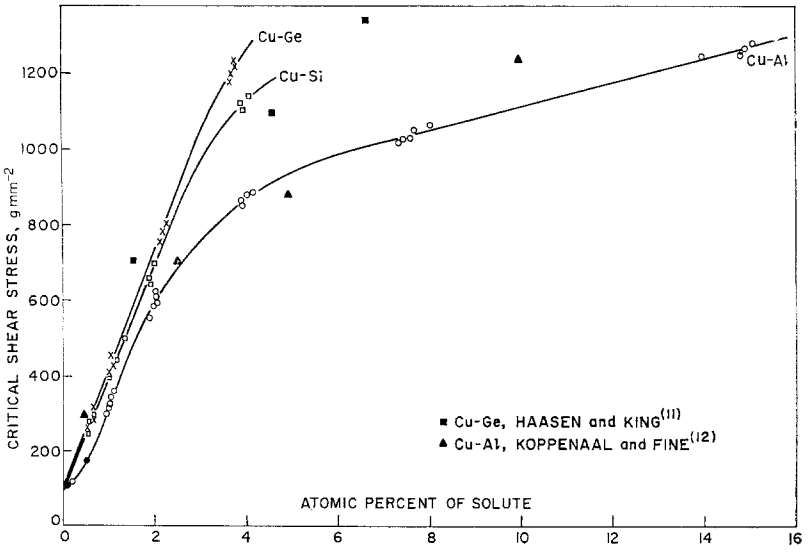

Figure 4 Effect of alloying on critical resolved shear stress for onset of plastic flow for various copper-base alloys (solid circles in Cu-Al series represent the average of three values).

[22] on Au-Ag alloys and Osswald [24] on Cu-Ni alloys, the data in Fig. 4 further show that for the three alloy systems S_0 increases at a decreasing rate with increasing solute content above about 2%. This behaviour appears to be typical of all fcc alloy systems at high concentrations [7, 9-11, 13, 24, 29]. Finally, it should be noted that for alloy concentrations between 0 and 2%, the critical shear stress increases at approximately the same rate for the three alloy systems. This is clearly demonstrated in Fig. 5, where the values of critical shear stress for the three alloy systems fall reasonably well on one line when plotted against *equivalent composition* (at. % solute element multiplied by its valency). Therefore, the marked difference in flow stress for the same alloy composition between Cu-Al crystals as compared to Cu-Ge and Cu-Si crystals can now be related to differences in the concentration of valency electrons. A similar effect was also obtained by Haasen and King [11] on plotting their S_0 data for Cu-Ge and Cu-Ga alloys against electron concentration. This dependency of S_0 on valency electron concentration in the present study is understandable, since the distortion in the immediate vicinity of any solute atom in a metal crystal is generally attributed not only to the relative size of the ionic radius of the solute atom, but also to the density of valence electrons around the solute atom; and as already indicated, the ionic radii of Al, Ge and Si are similar along with their electronegativity values. It follows, moreover, that the larger values of S_0 for the Cu-Ge and Cu-Si crystals as compared with the Cu-Al crystals for the same solute concentration can also be related to the lower solid solubility limits of Ge (12.0 at. %) and Si (11.6 at. %) in copper as compared with Al (20.4 at. %).

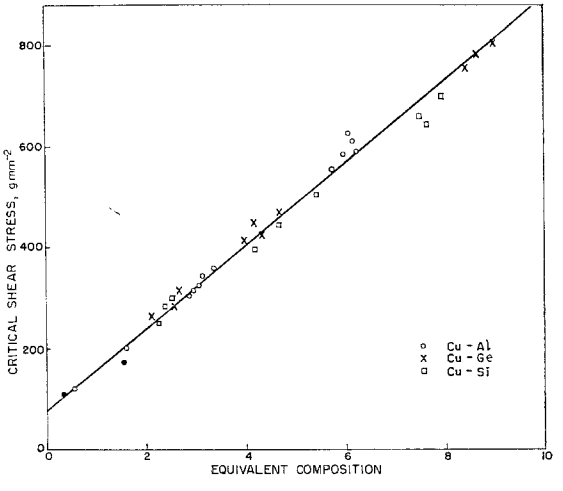

Figure 5 Dependence of critical resolved shear stress on equivalent composition of solute for various copper-base alloys.

3.2. Effect of orientation

Typical stress-strain curves for the Cu-Al, Cu-Ge and Cu-Si alloy crystals of different orientation

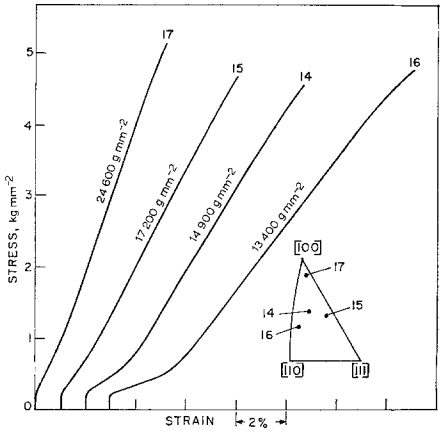

Figure 6 Stress-strain curves for Cu-0.2% Al alloy crystals of different orientation.

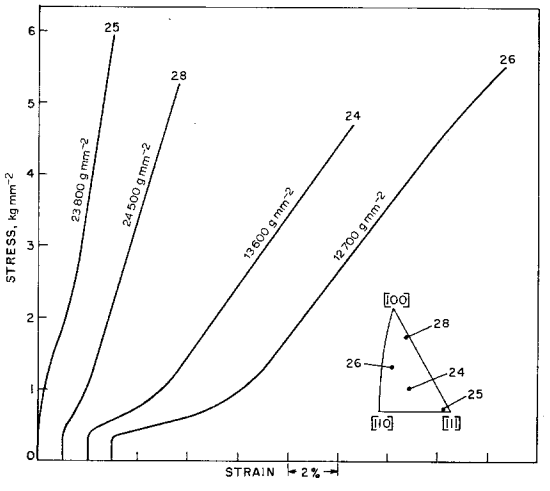

Figure 7 Stress-strain curves for Cu-0.5% Al alloy crystals of different orientation.

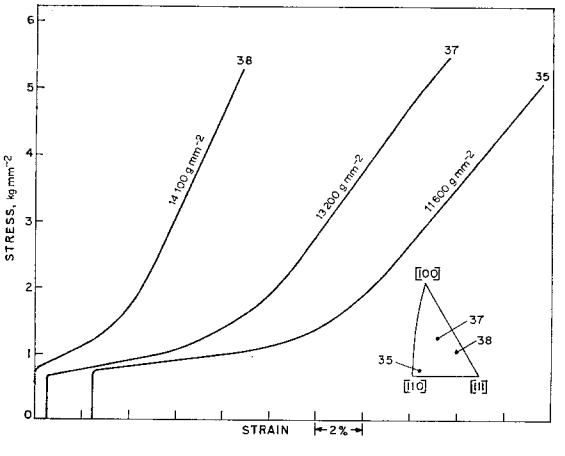

Figure 8 Stress-strain curves for Cu-1% Al alloy crystals of different orientation.

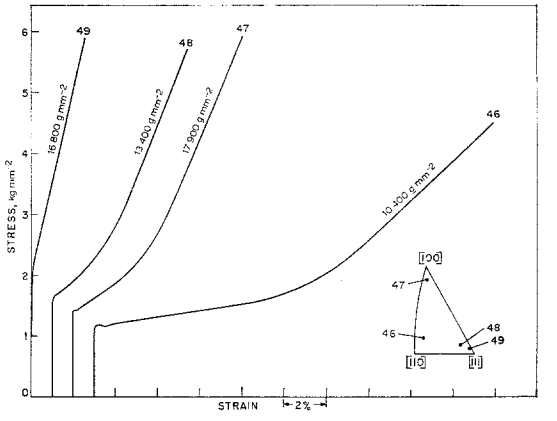

Figure 9 Stress-strain curves for Cu-2% Al alloy crystals of different orientation.

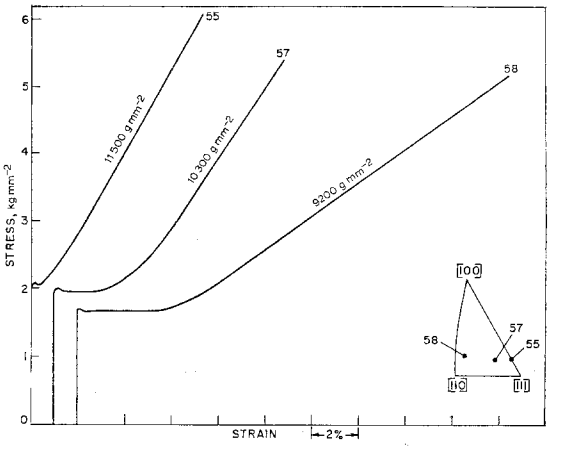

Figure 10 Stress-strain curves for Cu-4% Al alloy crystals of different orientation.

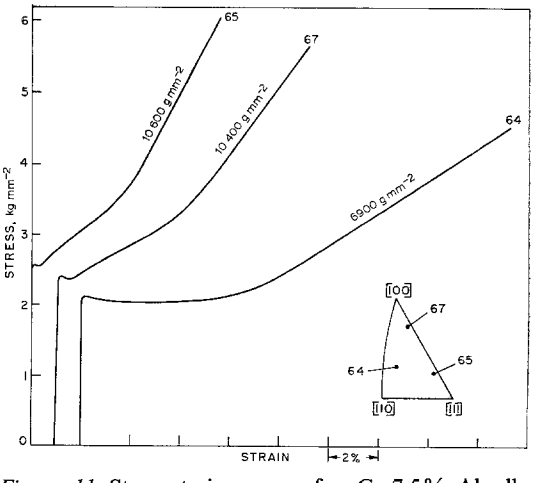

Figure 11 Stress-strain curves for Cu-7.5% Al alloy crystals of different orientation.

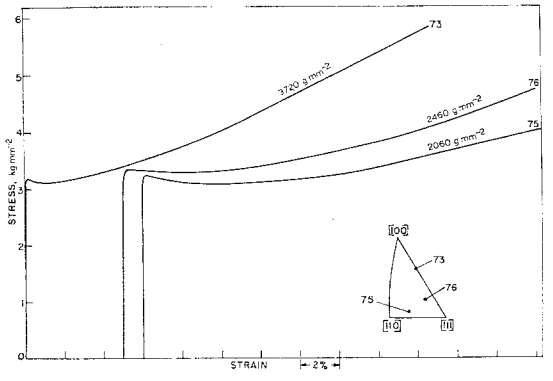

Figure 12 Stress-strain curves for Cu-15% Al alloy crystals of different orientation.

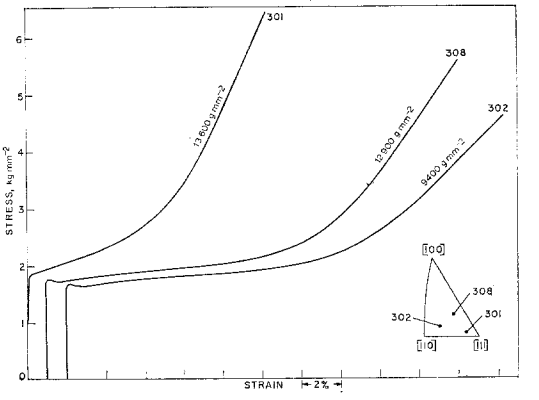

Figure 15 Stress-strain curves for Cu-2% Ge alloy crystals of different orientation.

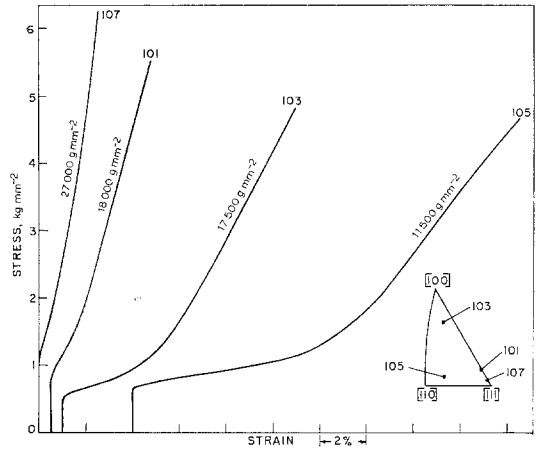

Figure 13 Stress-strain curves for Cu-0.5% Ge alloy crystals of different orientation.

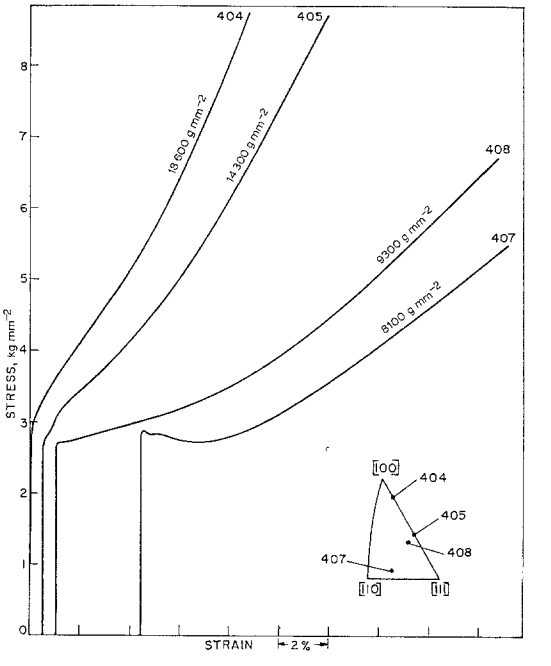

Figure 16 Stress-strain curves for Cu-4% Ge alloy crystals of different orientation.

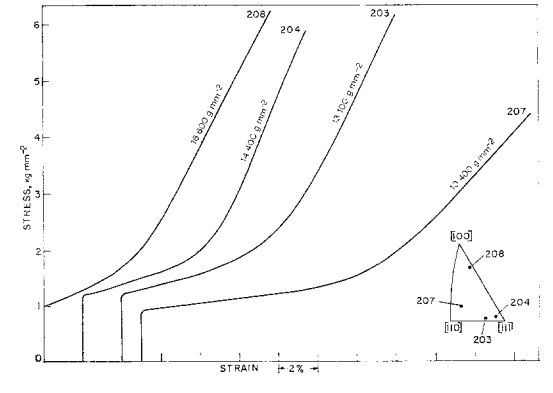

Figure 14 Stress-strain curves for Cu-1% Ge alloy crystals of different orientation.

at room temperature are shown in Figs. 6 to 18. These include alloys with solute concentrations ranging from 0.2 to 15% Al, 0.5 to 4% Ge and 0.6 to 2% Si. The original orientations of the crystals, which correspond to the tensile stress axis, are indicated in the accompanying standard stereographic triangles. It may be seen from Figs. 6 to 18 that the stress-strain curves for the alloys are of three general types as regards their gross shape. The first of these shows a high and approximately linear rate of strain-hardening immediately following the onset of plastic flow;

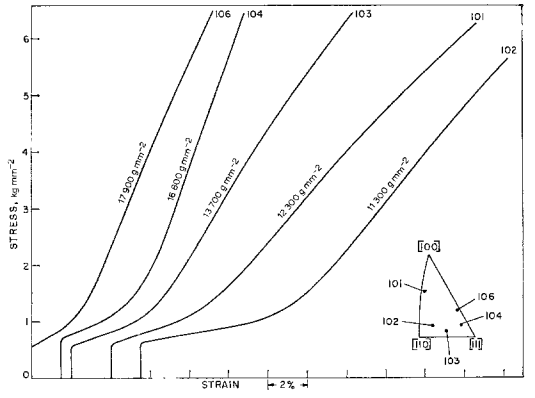

Figure 17 Stress-strain curves for Cu-0.6% Si alloy crystals of different orientation.

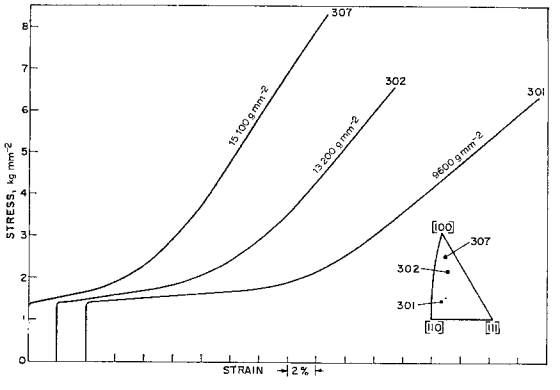

Figure 18 Stress-strain curves for Cu-2% Si alloy crystals of different orientation.

typical examples are crystals nos. 49 and 107 in Figs. 9 and 13, respectively. Stress-strain curves of this type are associated with crystals of low alloy content having initial orientations near the [100], [111] or the [100]-[111] boundary for duplex slip. One common feature of these critical orientations is the prediction of slip on more than one system at the start of plastic flow, and the maximum of four systems predicted for the [100] orientation has given the highest shear-hardening.

The second type of stress-strain curve displays the two-stage hardening process now commonly associated with face-centred cubic metal crystals and first examined in some detail in aluminium [31, 32], copper [33-35, 44, 45] and silver [33, 37] This type of curve is characterized by a low and linear rate of hardening or region of "easy glide" [37] followed by a region of much higher, but still linear, rate of hardening. Typical examples are the Cu-Al alloy crystals nos. 26 and 35 in Figs. 7 and 8, respectively; the Cu-Ge crystals nos. 105 and 207 in Figs. 13 and 14, respectively; and the Cu-Si crystals nos. 102 and 310 in Figs. 17 and 18, respectively. In general, those crystals exhibiting a distinct two-stage hardening curve have initial orientations which would predict extensive slip on a single (primary) system. It is noteworthy that in a few cases at large extensions the high rate of hardening in the second stage decreases with increasing strain, which suggests a tendency towards a parabolic rate of hardening reminiscent of the early observations in aluminium [47-49]. For the sake of convenience, and in consistency with standard terminology and a previous paper [33], the regions of low and high strain-hardening in the two-stage process will be designated hereafter as stages I and II, respectively. The coefficient of shear-hardening associated with stage II is indicated by the stress values on the curves.

The third type of stress-strain curve is essentially a modification of the two types discussed above, in that in addition to the single-stage or two-stage hardening process a double yield point [50, 51] is obtained, which is characterized by a decrease in stress with strain to provide an upper and lower yield point. This yield-point effect has been observed at room temperature by Piercy *et al* [3] and Mitchell and Thornton [15] in alpha-brass crystals, by Koppenaal and Fine [12] in Cu-Al crystals, and by Haasen and King [11] in Cu-Ge crystals. In the present work the first evidence of this yield-point phenomenon was observed in the Cu-2% Al (see Fig. 9) and Cu-2% Ge (see Fig. 15) crystals and only for those orientations well within the region of the stereographic triangle requiring slip on a single system (see crystals nos. 46 and 302). In this connection, however, it may be seen from the stress-strain curves in Figs. 10 and 11 that for alloys with an aluminium content of 4% or more, the double yield point is manifested in all crystals independent of their original orientation. This was not the case with the Cu-Ge crystals at these higher alloy concentrations. The Cu-Al crystals no. 55 in Fig. 10 and no. 46 in Fig. 9 are good examples of the occurrence of a double yield point followed by a single-stage and two-stage hardening process, respectively. It is particularly noteworthy that a double yield point was never observed in the stress-strain curves for the Cu-Si alloy crystals up to the highest concentration (2%) examined. A final observa-

tion of interest was the association of the lower yield point with relatively large values of strain, the so-called "yield-point elongation" region of Miller and Milligan [46]. Under the conditions of tensile testing this gives a region in the stress-strain curve of negative strain-hardening, or flow at constant stress, which replaces stage I in the two-stage hardening curve. In general, this phenomenon occurs only in crystals of high alloy content and with initial orientations predicting extensive slip on a single system. Typical examples are the Cu-Al and Cu-Ge crystals nos. 64 and 407 in Figs. 11 and 16, respectively, where the lower yield point occurs at strains of 3 to 4%.

It may be seen from Figs. 6 to 18 that for all of the alloys examined the nature of the stress-strain curve depends markedly on crystal orientation; and this dependence is very similar to that observed by the author in copper and silver [33]. The two-stage hardening curves for the Cu-Al alloys in Figs. 6 to 8, the Cu-Ge alloys in Figs. 13 and 14 and the Cu-Si alloys in Figs. 17 and 18 show that there is (1) a systematic decrease in the amount of strain associated with stage I and (2) an increase in the strain hardening of both stages I and II as the original orientation of the crystal goes from the [1 1 0] to the [1 0 0], [1 1 1], or [1 0 0] – [1 1 1] symmetry position; i.e. a decrease in χ_0. Since the probability for unpredictable slip or multiple glide to occur is greater on approaching such critical orientations, it would seem that the extent of stage I depends largely upon the complexity of the slip process immediately following the onset of flow in these alloy systems, as in the case of pure metal crystals. It is also apparent from the curves in Figs. 6 to 18 that the degree of shear-hardening associated with stage II is never greater than that for the single-stage hardening curves associated with slip on several systems at the onset of plastic flow; and in addition, the highest hardening is usually obtained in those crystals with orientations near the [1 0 0]. This is clearly shown by a comparison of the shear-hardening coefficients indicated on the curves for the Cu-Al crystals in Figs. 6, 7 and 9, and Cu-Ge crystals in Fig. 13. This high degree of linear shear-hardening, therefore, must be related to the multiplicity of glide and its pattern of intersecting slip lines. Hence, a possible explanation for the main source of this high hardening is the strain associated with piled-up dislocations at sessiles formed by coalescing edge dislocations on intersecting slip planes [52, 53].

As already indicated, there is also an orientation effect on the appearance of the yield-point phenomenon in these alloy crystals. An examination of Fig. 9 for Cu-2% Al crystals and Fig. 15 for Cu-2% Ge crystals clearly shows that a double yield point is favoured for orientations furthest removed from the [1 0 0] – [1 1 1] boundary associated with slip on more than one system. Furthermore, these same preferred orientations favour the appearance of an extensive "yield-point elongation" zone of negative or zero strain-hardening. Finally, it should be noted that the orientation effect on the amount of strain associated with stage I still persists in those high alloy crystals, which exhibit the yield-point phenomena at all crystal orientations.

The above observations on the effect of orientation in Cu-Al, Cu-Ge and Cu-Si crystals are not supported by the work of Piercy *et al* [3] in 70:30 brass crystals extended at room temperature. Their results show no significant differences in the shape of the stress-strain curve as regards the extent of stage I and the work-hardening in both stages I and II for a wide range of crystal orientations; and in these crystals, stages I and II appeared well-defined. More recently, Mitchell and Thornton [15] also reported no orientation effect in 80:20 and 70:30 brass crystals with regard to the low strain-hardening in stage I. However, they did find that the extent of easy glide in stage I and the linear work-hardening in stage II have the same orientation effects as those reported in the present work, but to a lesser degree. It would appear from a comparison of this earlier work with the present results that the effect of crystal orientation on the stress-strain characteristics of stages I and II becomes less pronounced in alloys of high solute concentration, where inhomogeneities in slip band development are so severe as to mask sophisticated orientation effects. This is supported by the heterogeneous formation and propagation of Lüders bands in stage I observed by Piercy *et al* [3], and the effect of this inhomogeneous deformation on the pattern of conjugate slip in stage II. In the Cu-Al, Cu-Ge and Cu-Si alloys of the present investigation no Lüders bands were observed during deformation. Instead, clustering of slip bands occurred, and uniformly along the entire gauge length of the crystals. This could reflect the comparatively lower solute concentrations in the alloy crystals of the present study in addition to the more homogeneous method of tensile deformation

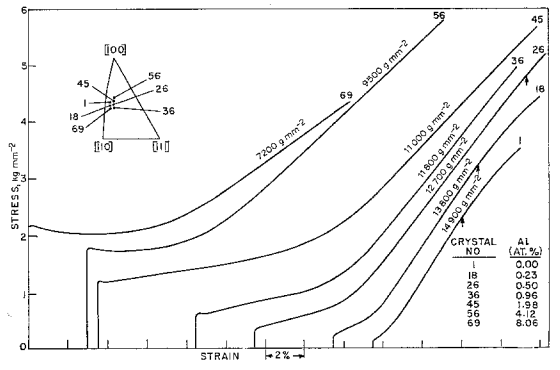

Figure 19 Effect of alloying on the stress-strain curves of Cu-Al alloy crystals of similar orientation.

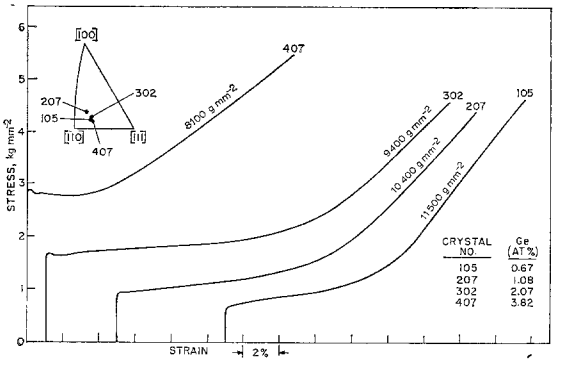

Figure 20 Effect of alloying on the stress-strain curves of Cu-Ge alloy crystals of similar orientation.

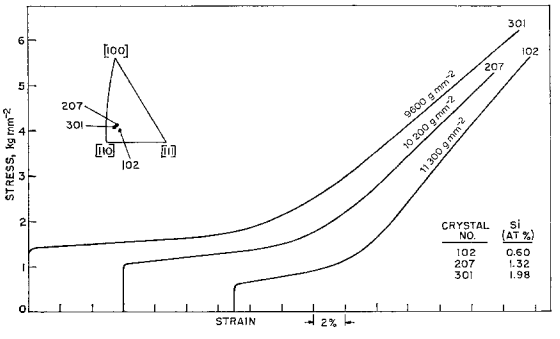

Figure 21 Effect of alloying on stress-strain curves of Cu-Si alloy crystals of similar orientation.

with the gimble-grip arrangement of Fig. 2.

3.3. Effect of alloying

Figs. 19 to 21 show the effect of solid-solution alloying on the gross shape of the stress-strain curve for the Cu-Al, Cu-Ge and Cu-Si crystals. To eliminate the orientation effect described in the previous section, crystals of similar orientation were used for each alloy system; and in addition, initial orientations were selected so as to provide a two-stage hardening process. The curves in Figs. 19 to 21 clearly show that an increase in alloying produces the following effects: (1) the critical resolved shear stress for plastic flow increases, as was already established by the data in Fig. 4; (2) the double yield-point phenomenon, which occurs only in the higher alloys of Cu-Al and Cu-Ge crystals, becomes more pronounced (upper yield stress minus lower yield stress) and eventually replaces stage I by a negative strain-hardening region under the conditions of tensile testing; (3) the extent or amount of shear associated with stage I increases; and (4) the shear-hardening coefficient for both stages I and II decreases. Again, the stress values indicated on the curves represent the shear-hardening coefficient for stage II. It follows from effects (3) and (4) that an increase in alloy content has the same general effect on the shape of the strain-hardening curve as when the initial orientation of a given alloy crystal goes from the [100], [111] or [100] – [111] boundary towards the [110]; i.e. an increase in χ_0 (see, for example, the orientation effect in Figs. 7 and 8). The stress-strain curves for the Cu-Al crystals, nos. 1, 18 and 26, in Fig. 19 also show that the amount of shear associated with the linear hardening of stage II increases with increasing alloy content, as well as the stress corresponding to the end of stage II or the point of deviation from linearity in the shear hardening (see arrows on curve).

Many of the above alloying effects on the stress-strain characteristics of face-centred cubic alloy crystals at room temperature were also observed in the early work of von Göler and Sachs [21] on Cu-Zn alloys, Sachs and Weerts [23] on Au-Ag alloys, Osswald [24] on Cu-Ni alloys, and more recently Jaoul [4] on Al-Cu and Al-Zn alloys, Meissner [10] and Mader [14] on Ni-Co alloys, Haasen and King [11] on Cu-Ge and Cu-Ga alloys, Koppenaal and Fine [12] on Cu-Al alloys, and Mitchell and Thornton [15] on Cu-Zn alloys. This is particularly true in the case of the dependence on alloying of the initial flow stress, the extent of stages I and II, and the stress associated with the end of stage II. There is also considerable agreement on the appearance of a yield-point effect with increasing alloy concentration for a number of Cu-base systems [11, 12, 15], although in the case of Co-Ni alloys

[10, 14] no double yield point was observed even in crystals with concentrations as high as 67% Co. However, there are major discrepancies in connection with the strain-hardening parameters in stages I and II. In both the Cu-Ga alloys [11] and Co-Ni alloys [10, 14] the rate of hardening in stage I was found to decrease with increasing solute concentration, whereas the strain-hardening in stage II was reported to be independent of alloying even for concentrations as high as 60% Co in the case of the Co-Ni crystals. Conversely, Mitchell and Thornton [15] observed no significant dependence of strain-hardening in stage I on alloying over a wide concentration in alpha-brass crystals, but they did find a marked decrease at room temperature in the linear strain-hardening of stage II with increasing zinc concentration. It is possible that some of this discrepancy with the results of the present work is due to the ill-defined nature of stage I, particularly in crystals of high alloy concentration. However, it is more likely that it is a result of the failure in previous studies to completely eliminate the effect of crystal orientation in examining alloying effects; and the stress-strain curves of Figs. 6 to 18 give ample evidence that over a wide range of alloy concentration this orientation parameter has a significant effect on all the stress-strain characteristics of stages I and II, with the sole exception of the critical shear stress for the onset of plastic flow. It is further possible that the method of tensile testing and crystal dimensions are also reflected in this data comparison, as they may affect slip line development.

In the case of the Cu-Ge crystal no. 407 in Fig. 20, it is interesting to note the tendency towards a discontinuous or repetitive yielding immediately following the advent of plastic flow, which is manifested by the occurrence of successive double yield points. This discontinuous yielding, as well as the mechanical effect of a double yield point, have been generally associated in metals and alloys with strain-ageing phenomena due to anchoring of dislocations by impurity or solute atoms in the manner proposed by Cottrell [2, 50, 51]. According to this mechanism the yield-point phenomenon is identified by the following chracteristics: (1) the yield point exhibits an upper and lower yield stress, or a yield-point elongation zone (flow at constant stress), both of which were observed in the curves of Fig. 10 for Cu-4% Al crystals; (2) on immediately reloading a specimen which had been plastically strained, there is a smooth transition from the elastic to the plastic regions of the stress-strain curve instead of the yield phenomenon described in (1); and (3) on annealing a pre-strained specimen (strain-anneal), the double yield point returns.

In an effort to establish the existence of the yield phenomenon in accordance with the above criteria, the following experiment was conducted and the results are summarized in Fig. 22. A

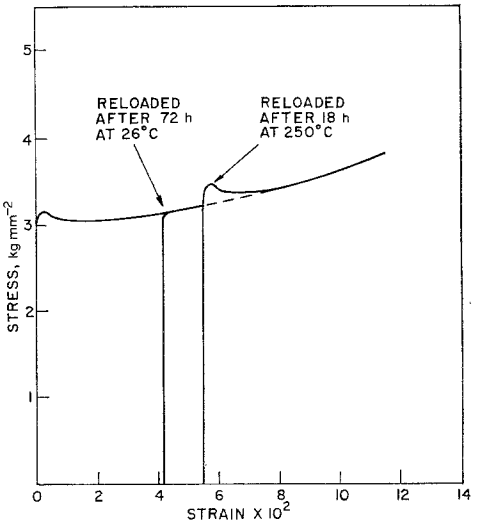

Figure 22 Effect of pre-strain and anneal on stress-strain curve for a Cu-15% Al alloy crystal.

Cu-Al alloy crystal was initially stressed at room temperature to a strain of approximately 4%. The alloy content (15% Al) and original orientation (near [1 1 0]) of the crystal were selected to insure occurrence of a double yield point on initial loading. Following the prestrain of 4%, the crystal was immediately reloaded at 26°C, strained an additional 1.5%, and then given an anneal at 250°C in a purified helium atmosphere for 18 h at zero load. Immediately after this strain-anneal treatment, the specimen was again reloaded at 26°C to a total strain of approximately 12%. It may be seen from the stress-strain diagrams in Fig. 22 that the initial loading at 26°C did produce a double yield point, which disappeared immediately upon reloading after the initial strain of 0.04. It is further evident that upon reloading after the anneal at 250°C, the yield-point phenomenon returned and was even more pronounced (upper − lower yield stress). Similar behaviour was observed by Piercy *et al*

TABLE I Data on the two-stage hardening curves for Cu-Al alloy crystals: S_I = critical resolved shear stress (onset of stage I); S_{II} = resolved shear stress (onset of stage II); a_I = shear strain (extent of stage I); $(\tau/a)_I$ = shear-hardening coefficient of stage I

Crystal no.	Al (at. %)	S_I (g mm^{-2})	S_{II} (g mm^{-2})	S_{II}-S_I (g mm^{-2})	a_I	$(\tau/a)_I$ (g mm^{-2})
CA 14	0.20	120	290	170	0.030	5670
CA 16	0.16	115	288	173	0.050	3460
CA 18	0.23	129	314	185	0.052	3560
CA 19	0.19	121	285	164	0.032	5130
Av.	0.20	121	294	173		
CA 24	0.54	203	448	245	0.058	4220
CA 26	0.50	176	413	237	0.096	2470
CA 27	0.53	185	449	264	0.084	3140
CA 28	0.53	194	444	250	0.022	11400
CA 29	0.55	208	478	270	0.088	3070
Av.	0.53	193	446	253		
CA 35	1.03	324	627	303	0.210	1440
CA 36	0.96	300	601	301	0.148	2030
CA 37	1.05	331	652	319	0.167	1910
CA 38	1.01	322	619	297	0.092	3230
CA 39	1.09	355	668	313	0.206	1520
Av.	1.03	326	633	307		
CA 45	1.98	577	938	361	0.221	1630
CA 46	1.82	535	884	349	0.205	1700
CA 47	2.04	626	997	371	0.077	2070
CA 48	2.02	610	865	255	0.065	2540
Av.	1.97	587	921	334		

TABLE II Data on the two-stage hardening curves for Cu-Ge alloy crystals: S_I = critical resolved shear stress (onset of stage I); S_{II} = resolved shear stress (onset of stage II); a_I = shear strain (extent of stage I); $(\tau/a)_I$ = shear-hardening coefficient of stage I

Crystal no.	Ge (at. %)	S_I (g mm^{-2})	S_{II} (g mm^{-2})	S_{II}-S_I (g mm^{-2})	a_I	$(\tau/a)_I$ (g mm^{-2})
CG 101	0.66	314	586	272	0.032	8500
CG 103	0.51	263	523	260	0.089	2920
CG 104	0.54	268	542	274	0.129	2120
CG 105	0.67	317	594	277	0.175	1580
CG 106	0.60	284	542	258	0.176	1470
CG 108	0.65	302	588	286	0.060	4770
Av.	0.61	291	562	271		
CG 201	1.18	465	801	336	0.204	1650
CG 202	1.01	422	732	310	0.258	1200
CG 203	1.21	494	825	331	0.195	1700
CG 204	1.05	449	745	296	0.181	1630
CG 206	0.95	401	695	294	0.276	1070
CG 207	1.08	440	743	303	0.232	1310
CG 208	1.14	464	787	323	0.096	3360
Av.	1.09	448	761	313		
CG 301	1.98	704	1078	374	0.186	2010
CG 305	2.24	788	1170	382	0.354	1100
CG 308	2.14	774	1138	364	0.300	1210
CG 309	2.02	719	1079	360	0.281	1280
CG 310	2.18	770	1153	383	0.121	3160
Av.	2.11	751	1124	373		

TABLE III Data on the two-stage hardening curves for Cu-Si alloy crystals: S_I = critical resolved shear stress (onset of stage I); S_{II} = resolved shear stress (onset of stage II); a_I = shear strain (extent of stage I); $(\tau/a)_I$ = shear-hardening coefficient of stage I

Crystal no.	Si (at. %)	S_I (g mm^{-2})	S_{II} (g mm^{-2})	S_{II}-S_I (g mm^{-2})	a_I	$(\tau/a)_I$ (g mm^{-2})
CS 101	0.63	307	584	277	0.098	2830
CS 102	0.60	290	561	271	0.181	1580
CS 103	0.57	269	530	261	0.093	2810
CS 104	0.58	276	534	258	0.111	2330
CS 106	0.55	252	504	252	0.049	5150
Av.	0.59	281	545	264		
CS 201	1.37	524	863	339	0.247	1370
CS 202	1.29	505	824	319	0.181	1760
CS 203	1.00	378	684	306	0.162	1890
CS 204	1.14	441	754	313	0.149	2100
CS 207	1.32	517	841	324	0.243	1330
Av.	1.22	473	793	320		
CS 301	1.98	690	1045	355	0.301	1180
CS 302	1.94	684	1050	364	0.246	1480
CS 304	2.01	704	1082	378	0.240	1570
CS 307	1.85	640	1000	360	0.179	2010
Av.	1.95	680	1044	364		

[3] on strain-annealing 70:30 brass crystals at 200°C for 2 h at room temperature. The dashed line in Fig. 22 represents the shape of the stress-strain curve in the absence of interruptions in the loading, which was determined by stressing a crystal grown from the same seed and, hence, with identical orientation and alloy content as the crystal in Fig. 22. It would appear from these results that the yield point phenomenon observed in the Cu-Al and Cu-Ge crystals can be interpreted in accordance with the Cottrell mechanism of yielding.

The data pertinent to the evaluation of the two-stage hardening curves for the various alloys in the Cu-Al, Cu-Ge and Cu-Si systems are given in Tables I to III. Included in the Tables are the values of critical resolved shear stress for the onset of stage I, S_I, the increment of shear stress associated with stage I, S_{II}-S_I, the shear strain corresponding to the end of stage I, a_I, and the shear-hardening coefficient of stage I, $(\tau/a)_I$. These are the same parameters (see Fig. 23) which are adopted in a previous work [32] to define the stress-strain curve on examining the orientation effect in pure metal crystals; and again the co-ordinates, S_{II} and a_I, were obtained from the intersection of the two linear regions of the two-stage hardening curves. The values of the shear hardening coefficient for stage II, $(\tau/a)_{II}$, are not included in Tables I to III, since

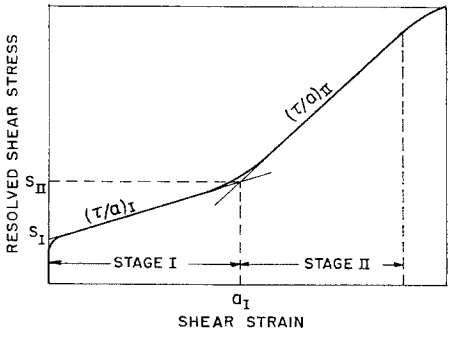

Figure 23 Schematic representation of stress-strain parameters defining two-stage hardening curve: S_I – critical resolved shear stress for onset of stage I; S_{II} – critical resolved shear stress for onset of stage II; a_I – shear strain associated with extent of stage I; $(\tau/a)_I$ – shear-hardening coefficient of stage I; $(\tau/a)_{II}$ – shear-hardening coefficient of stage II.

these are indicated on all of the stress-strain curves. In compiling the data in Tables I to III, only those crystals were included whose initial orientation and/or alloy content resulted in a well-defined two-stage hardening curve, and exhibited no yield-point elongation zone at constant stress or negative hardening. The nature of this yield point effect does not permit a reliable estimate of the value of a_I.

It is apparent from the data in Tables I to III

that for each composition in the three alloy systems the values of a_I and (τ/a_I) are markedly dependent upon orientation, as indicated earlier. Thus, the effect of crystal orientation on these two parameters persists regardless of the degree of alloying. However, the co-ordinate of shear stress, S_{II}, is not dependent upon orientation for a given alloy composition, if one takes into account the variations in alloy content from the indicated mean value for each alloy. Thus, like S_I, it would appear that the value of resolved shear stress for the onset of stage II is associated with a critical resolved shear stress law for the alloys examined. It follows, therefore, that stage I is associated with an increment of shear stress, $S_{II} - S_I$, which for each alloy is also independent of crystal orientation and, hence, on the amount of shear of stage I, a_I. These generalizations are in agreement with the earlier work [33] on characterizing the two-stage hardening curve for silver, copper, and aluminium single crystals, and later confirmed by Garstone *et al* [35] for copper crystals.

It is also apparent from Tables I to III that S_{II} increases markedly with alloying, and at a more rapid rate than S_I. This is clearly indicated in Fig. 24, which shows the dependence of the stress increment, $S_{II} - S_I$, on alloying for Cu-Al, Cu-Ge, and Cu-Si crystals of different orientation. Since the onset of stage II is associated with the occurrence of unpredicted slip on a secondary system, then the pinning by solute atoms of those dislocations responsible for flow on this system must also become more effective with alloying. Stated another way, with increasing solute concentration larger stress fields of dislocation pile-ups due to primary slip are required in order to activate movement of dislocations on secondary systems.

It is further apparent from Fig. 24 that $S_{II} - S_I$ increases with alloy content at a decreasing rate, as in the case of S_I (see Fig. 4). The fact that the scatter in the data falls on the generalized curve within experimental error is again a clear manifestation of the invariance of S_{II} on crystal orientation for the alloys examined in the three systems. A similar increase in S_{II} with alloy concentration was obtained in Cu-Ge crystals by Haasen and King [11], who also showed a decrease in the ratio S_{II}/S_I with increasing alloy content similar to that found in the present study. In fact, their S_{II}/S_I values of 1.6 to 1.7 for 1.4% Ge crystals at 295 K compare very favourably with the values of 1.70 for Cu-1.1% Ge crystals, 1.68 for Cu-1.2% Si crystals, and 1.56 for the Cu-2% Al crystals obtained from the data in Tables I to III.

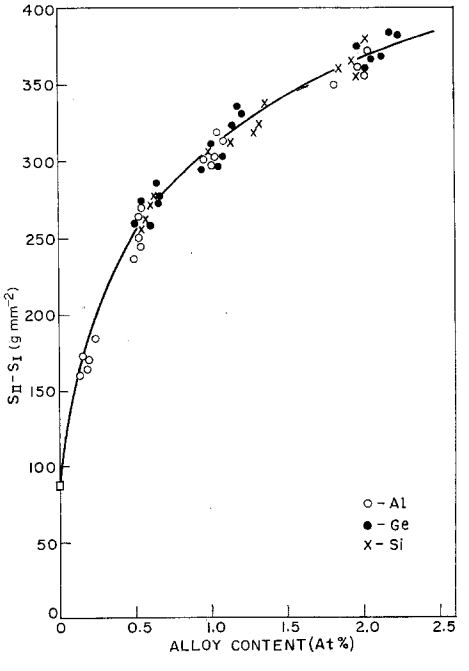

Figure 24 Variation in the increment of shear stress (S_{II}-S_I) with alloying in Cu-Al, Cu-Ge and Cu-Si crystals of different orientation.

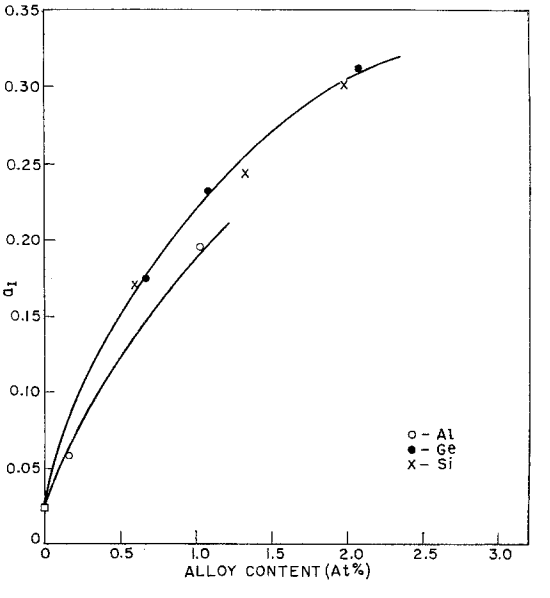

Figure 25 Effect of alloying on shear strain associated with extent of stage I (a_I) for Cu-Al, Cu-Ge and Cu-Si crystals of similar orientation.

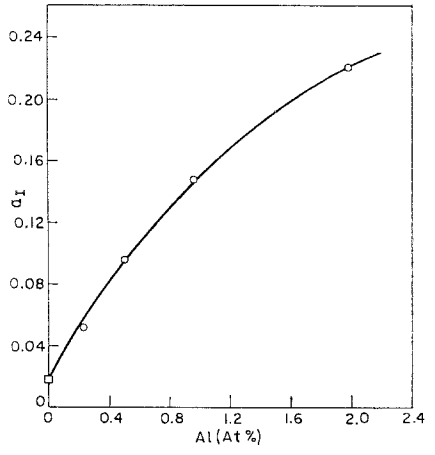

Figure 26 Effect of alloying on shear strain associated with extent of stage I (a_I) for Cu-Al crystals of similar orientation, but different from that of crystals in Fig. 25.

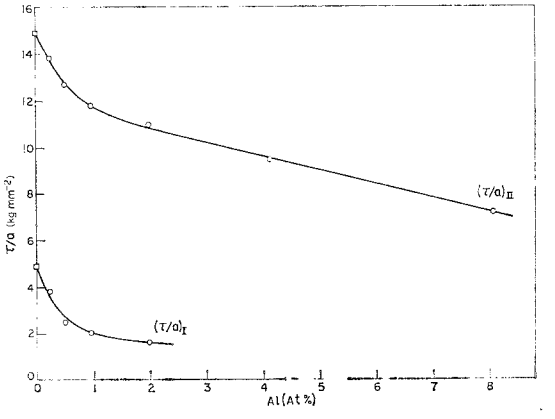

Figure 27 Effect of alloying on shear hardening coefficient of stage I, $(\tau/a)_I$, and stage II, $(\tau/a)_{II}$, for Cu-Al crystals of similar orientation.

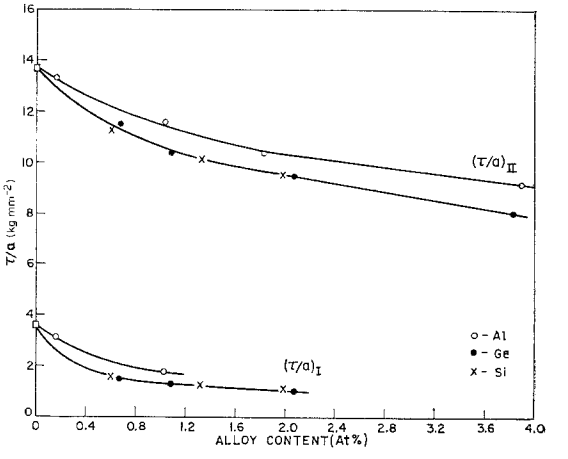

Figure 28 Effect of alloying on shear hardening coefficient of stage I, $(\tau/a)_I$, and stage II, $(\tau/a)_{II}$, for Cu-Al, Cu-Ge and Cu-Si crystals of similar orientation.

The curves in Fig. 25 summarize the effect of alloying on the shear strain (a_I) associated with stage I for Cu-Al, Cu-Ge and Cu-Si crystals of similar orientation; and Fig. 26 provides the same but more detailed data for only Cu-Al crystals of similar orientation, but different from that of the alloys in Fig. 25. As was already indicated qualitatively by the stress-strain curves of Figs. 19 to 21, the value of a_I increases markedly with alloying; and the general form of this dependence is very similar to that of $S_{II} - S_I$ on alloying. It may also be seen from Fig. 25 that the Cu-Ge and Cu-Si crystals give a very similar dependence of a_I on alloying, with a_I increasing from a value of ~ 0.025 for pure Cu of similar orientation to ~ 0.30 for the 2% alloy. On the other hand the Cu-Al system gives somewhat lower values of a_I for a given alloy content; and in this connection, it should be noted from Figs. 4 and 24 that for a given alloy composition the values of S_I and S_{II} also tend to be lower for the Cu-Al system.

The nature of the variation in the shear-hardening coefficients for stage I, $(\tau/a)_I$, and stage II, $(\tau/a)_{II}$, with alloying is shown in Figs. 27 and 28 for crystals of similar orientation in the three alloy systems. The curves give striking evidence of the much higher shear-hardening in stage II of the stress-strain curves for the alloys examined; and it may be seen that both $(\tau/a)_I$ and $(\tau/a)_{II}$ decrease markedly with increasing alloy content, but at a decreasing rate. Hence, this dependence is just the converse of that for $S_{II} - S_I$ and a_I on alloying. A comparison of the curves for the three alloy systems in Fig. 28 again shows similar behaviour for the alloys in the Cu-Ge and Cu-Si systems, whereas the Cu-Al alloys have significantly higher values of both $(\tau/a)_I$ and $(\tau/a)_{II}$ for the same alloy content. A comparison of Figs. 25 and 28 clearly show that for similar orientations higher values of shear strain (a_I) are associated with lower values of shear-hardening coefficients in both stages I and II for all alloy crystals in the three systems.

The effect of the nature of the solute on the stress-strain curve was examined by selecting crystals in the three systems with similar alloy content and orientation. The results are summarized in Figs. 29 to 31, where again the stress

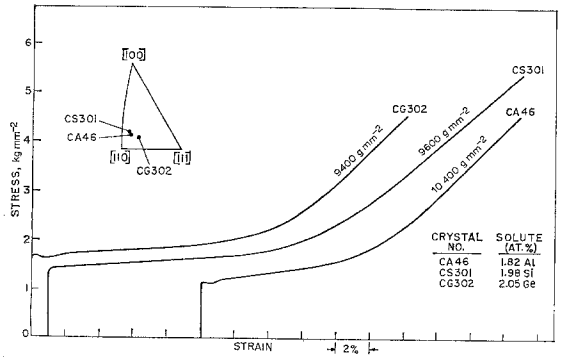

Figure 29 Stress-strain curves for Cu-Al, Cu-Ge and Cu-Si crystals of similar alloy content and orientation.

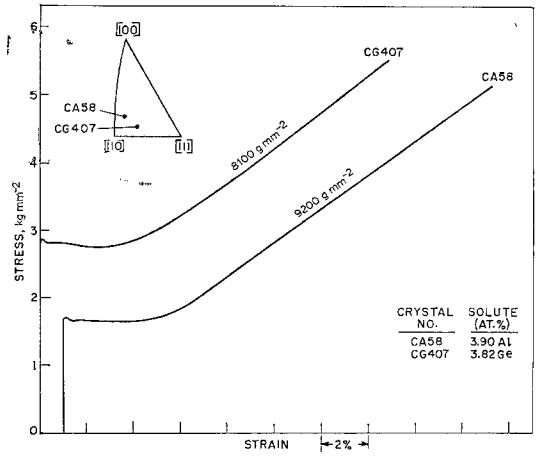

Figure 30 Stress-strain curves for Cu-Al and Cu-Ge crystals of similar alloy content and orientation.

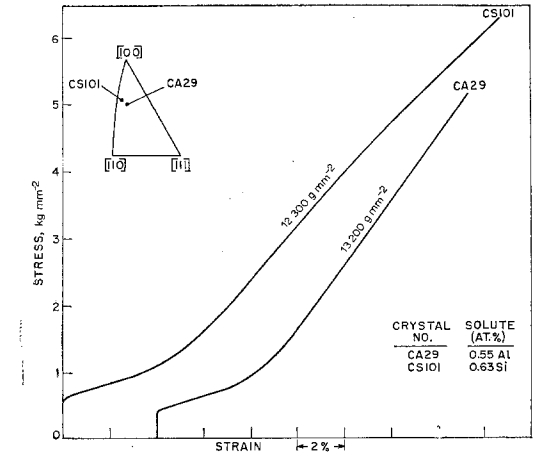

Figure 31 Stress-strain curves for Cu-Al and Cu-Si crystals of similar alloy content and orientation.

values indicated on the curves represent the shear-hardening coefficient for stage II. In Fig. 29 are shown the curves for Cu-Al, Cu-Ge and Cu-Si crystals, and again one striking difference in their shape is the absence of a double yield point in the case of the Cu-Si crystal. Except for this difference, however, the nature of the Cu-Ge and Cu-Si curves are very similar in that they exhibit similar shear-hardening coefficients for both stages I and II. A comparison between the Cu-Al and Cu-Ge curves shows that for the Cu-Ge crystal the double yield point is somewhat more pronounced, stage I is extended to larger values of strain, and the shear-hardening in both stages I and II are lower. These general features are also manifested by the stress-strain curves in Fig. 30 for Cu-Al and Cu-Ge crystals of higher alloy content, but with initial orientations similar to the crystals in Fig. 29; here, however, the extent of stage I is difficult to evaluate because of the negative hardening in crystal CG 407. In Fig. 31 are shown the stress-strain curves for Cu-Al and Cu-Si crystals with a sufficiently low alloy content to avoid the occurrence of a double yield point, but with an initial orientation to provide a well-defined two-stage hardening curve. It may be seen that the addition of silicon to copper, as compared to aluminium, results in a greater yield stress, a larger strain associated with stage I, and a lower shear-hardening in both stages I and II.

In summary, it would appear from the curves in Figs. 29 to 31 that the substitution of germanium or silicon for aluminium as a solute in copper has the same general effect on the stress-strain diagram as (1) an increase in alloy content for a given solute and crystal orientation and (2) an increase in the value of χ_0 for a given alloy composition.

3.4. Slip line observations

The development of slip markings were optically examined on electrolytically polished surfaces of a number of Cu-Al crystals, whose initial orientations (Fig. 32) adequately cover the stereographic triangle, and include some near the [111], [110] and the [100] – [111] symmetry position. The range of compositions provided by these crystals is 0.2 to 8 % Al.

In those crystals, nos. 1, 2, 3, 5 and 6, which exhibit a two-stage hardening curve, the low hardening of stage I was associated with slip on a single (primary) system, while the onset of stage II was accompanied by the appearance of

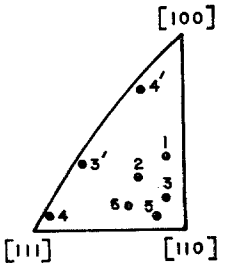

Figure 32 Original orientations of Cu-Al crystals used to study development of slip lines.

unpredictable slip on several systems. This was reported earlier for pure copper [33] and later confirmed by a number of investigators whose work is summarized in the reviews by Clarebrough and Hargreaves [25] and Mitchell [26]. It was also observed that the slip markings in stage I were uniformly distributed along the entire length of the crystal for all alloy concentrations examined, unlike the highly inhomogeneous propagation of Lüders bands observed by Piercy *et al* [3] during the extension of 70:30 brass crystals. With increasing alloy content there was also a definite tendency for the slip markings in stage I to cluster into distinct bands with increasing deformation, as was first reported for alpha brass crystals [20, 21]. This characteristic would have to account for the observed decrease in the low linear hardening of stage I with increasing alloy content. Finally, it was found that the high linear hardening of stage II in these crystals was associated predominantly with increased secondary slip on the conjugate system, although highly localized evidence of cross-slip in the form of bands was also observed. Examples of the above slip patterns in stages I and II are shown in Figs. 33 to 40.

The micrographs in Fig. 33 show the nature of the slip process in Cu-0.5% Al crystal no. 2, whose original orientation predicts extensive slip on a single system. Fig. 33a illustrates the uniform distribution of primary slip markings along the length of the crystal in stage I after 1.4% extension, while Figs. 33b and c show the characteristic appearance of secondary slip on the conjugate and cross slip planes in stage II after 2.8 and 4.2% extension, respectively. The uniform distribution of slip markings in stage I is also clearly manifested in the more dilute Cu-0.2% Al crystal no. 1 in Fig. 34.

Cu-1% Al crystal no. 3, which was extended

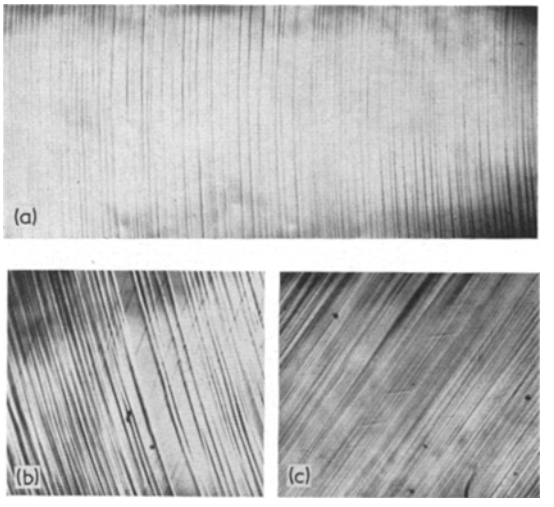

Figure 33 Slip-line pattern in stages I and II for Cu-0.5% Al crystal no. 2 with increasing extension, × 100. (a) Primary slip in stage I, 1.4% extension. (b) Conjugate slip in stage II, 2.8% extension (c) Cross-slip in stage II, 4.2% extension.

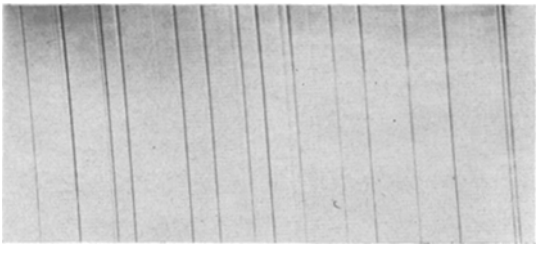

Figure 34 Uniform distribution of primary slip in stage I for Cu-0.2% Al crystal no. 1 after 0.6% extension, × 150.

up to 16% in stage II, also reveals the appearance of localized cross-slip in bands at a slight angle to the primary octahedral slip markings (see Fig. 35a). In addition there are also regions of the crystal where a few bands are seen with a characteristically rumpled appearance, as shown in Fig. 35b. Close examination reveals that many of the lines in these bands correspond to segments of conjugate slip as well as cross-slip, which is clearly indicated in the band on the right in the figure. Therefore, these rumpled bands are due to alternate slip on these secondary systems, in agreement with the earlier observations on aluminium [53] and copper [33].

Fig. 36 shows the development of slip markings with increasing deformation in Cu-4% Al crystal no. 5, whose original orientation is close to the [1 1 0]. The range of deformation shown is

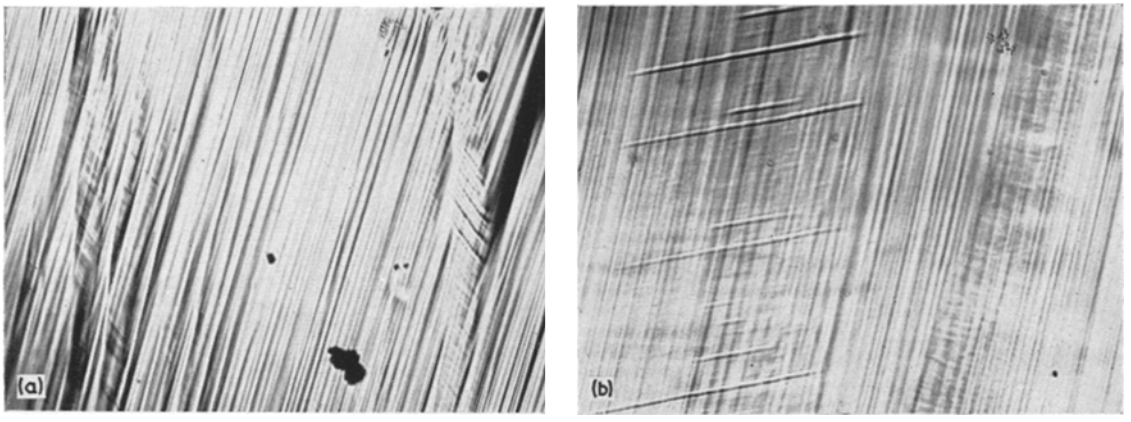

Figure 35 Localized nature of secondary slip in stage II in Cu-1% Al crystal no. 3. (a) Cross-slip after 10% extension × 100; (b) cross-slip and "rumpled" bands after 13% extension, × 130.

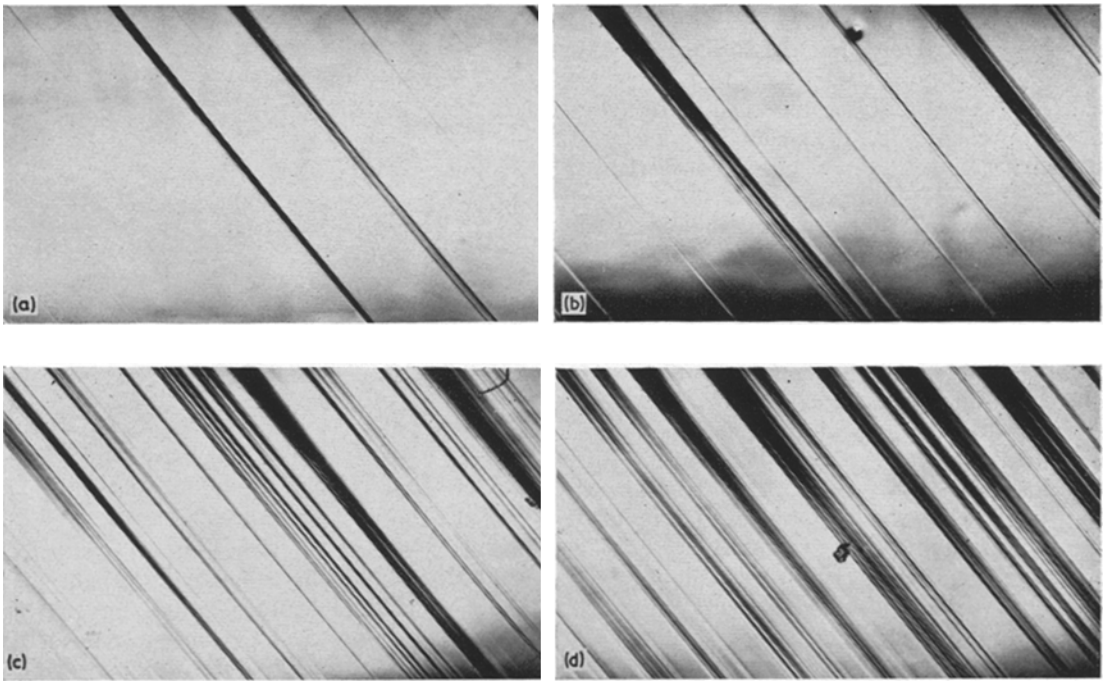

Figure 36 Development of slip bands with increasing deformation in stage I for Cu-4% Al crystal no. 5, × 100. (a) 0.2% extension, (b) 0.6% extension, (c) 1.1% extension, (d) 2% extension.

still within the region of stage I. One sees from the micrographs that slip occurs solely on the primary plane, and the slip lines tend to cluster into bands with increasing elongation, as contrasted to Fig. 33a and Fig. 34 for the more dilute alloy crystals, nos 1 and 2. Nevertheless, this preferential banding of slip markings does take place uniformly along the length of the crystal. Fig. 37 shows a region of crystal no. 5 exhibiting simultaneous slip on the primary, conjugate and cross-slip planes in stage II after 6.5% extension, which provides a pattern of many intersecting lines. However, with increasing deformation there is a tendency for the secondary slip to confine itself between bands of primary slip in these higher alloy crystals.

The micrographs in Fig. 38 show slip-band formation with increasing deformation in Cu-7.5% Al crystal no. 6, which exhibited a pronounced double yield point and whose orientation

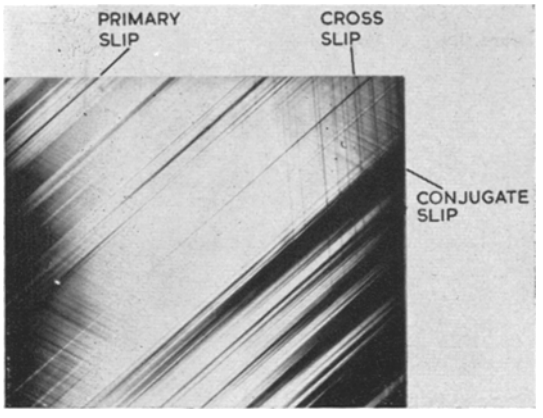

Figure 37 Multiple glide in Cu-4% Al crystal no. 5 after 4% extension in stage II, × 100.

is similar to crystal no. 5. The clustering of slip markings into bands with increased deformation is here even more evident. It also should be noted that in this crystal small segments of unpredicted cross-slip were observed within the bands of primary slip (see Fig. 39), suggesting that cross-slip promotes the continued clustering of slip markings with deformation.

In addition to the above crystals with two-stage hardening curves, a study was made of slip-band development in crystals with initial orientations predicting slip on two or more systems and exhibiting a single stage of high hardening. The micrograph in Fig. 40 shows a classical example of the occurrence of duplex slip on the primary and conjugate planes at the onset of plastic flow in Cu-1% Al crystal no. 3′. This uniform network of intersecting slip lines is typical of crystals whose original orientations are close to the [100] – [111] symmetry position. A similar slip band pattern was observed for Cu-2% Al crystal no. 4′.

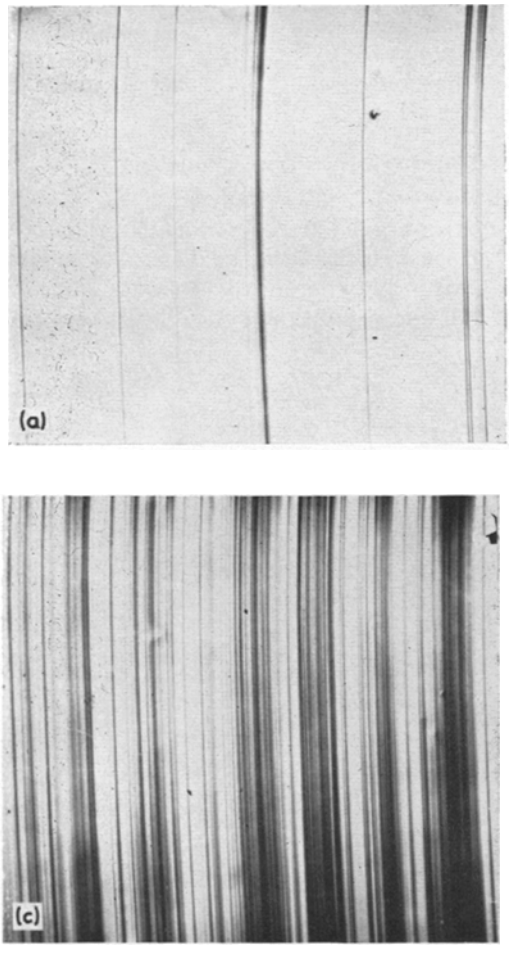

Figure 38 Development of slip bands with increasing deformation in stage I for Cu-7.5% Al crystal no. 6, × 100. (a) 0.3% extension, (b) 1% extension, (c) 3% extension.

Cu-2% Al crystal no. 4, whose orientation is close to the [111], also exhibited multiple glide at the onset of plastic flow. Here extensive slip on the primary, conjugate and cross-slip planes was observed. However, unlike the uniform network of intersecting slip lines associated with orientations near the [100] – [111] position (see Fig. 40), the secondary slip occurred predominantly between primary slip bands, and occasionally within the bands themselves. This is clearly indicated in the micrographs of Fig. 41 for the case of cross-slip, although a similar pattern was also observed for conjugate slip.

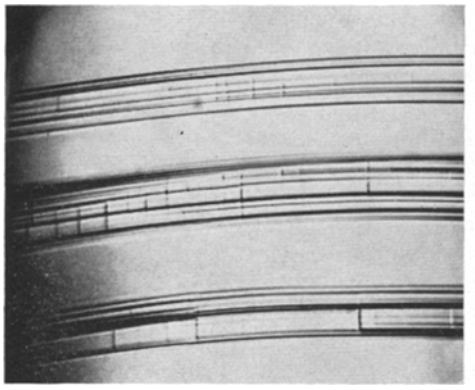

Figure 39 Appearance of cross-slip segments within bands of primary slip in Cu-7.5% Al crystal no. 6, × 250.

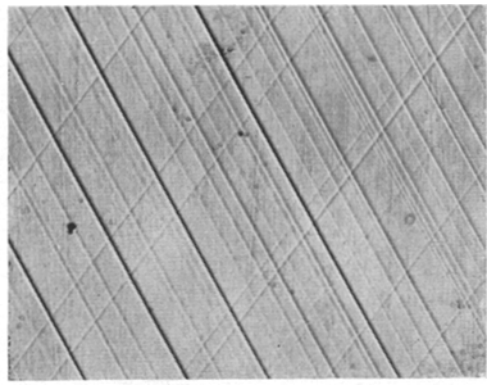

Figure 40 Primary and conjugate slip in Cu-1% Al crystal no. 3′ after 0.3% extension, × 100.

Fig. 41 also shows faint markings of conjugate slip within the primary band at the lower right-hand corner of the micrograph. Finally, Fig. 42 gives a good example of the inhibiting effect of cross-slip on the propagation of primary slip bands in crystal no. 4, and further serves to demonstrate the tendency of even cross-slip markings to cluster into bands.

In none of the crystals examined (Fig. 32), was any evidence of twinning or kink bands found. However, it should be noted that the maximum elongation was 16%, which was still within the range of linear hardening associated with stage II. The observation of mechanical twinning on the {111} ⟨121⟩ system by Haasen and King [11] in Cu-Ge and Cu-Ga crystals of high alloy content was for extensions beyond stage II and into the stress-strain region generally referred to as stage III.

4. Conclusions

4.1. Effect of orientation

1. A strong orientation-dependence was observed of the gross shape of the shear stress/shear strain diagram in all of the alloy crystals examined. For crystal orientations near the [100], [111] or

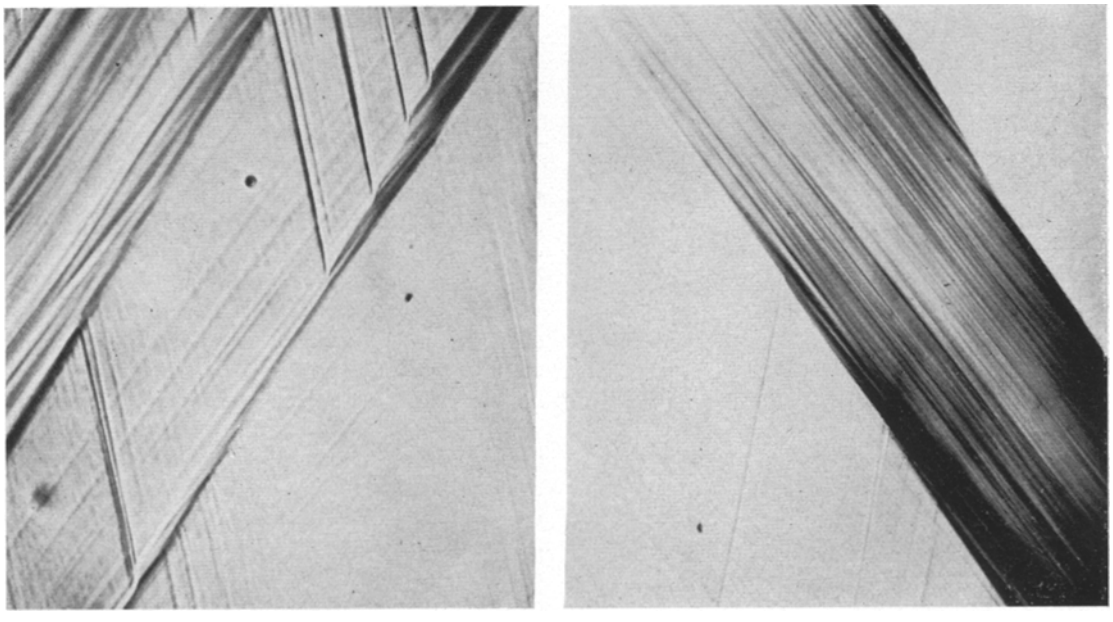

Figure 41 Examples of cross-slip between bands of primary slip in Cu-2% Al crystal no. 4 after 1.5% extension, × 150.

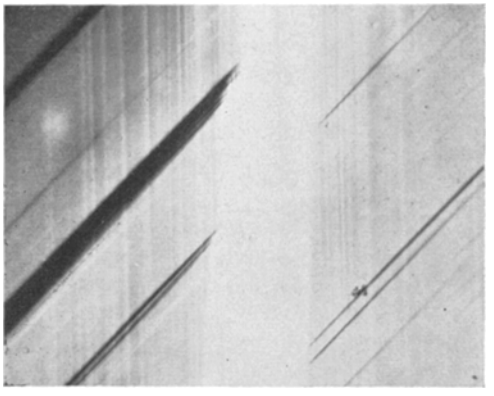

Figure 42 Clustering of cross-slip into bands and their inhibiting effect on the propagation of primary slip band in Cu-2% Al crystal no. 4 after 2% extension, × 130.

[100] – [111] boundary, the stress-strain diagram exhibits a high linear rate of hardening following the onset of plastic flow, whereas for orientations well removed from these critical orientations and near the [110], the typical two-stage hardening curve is obtained which is characterized by a low linear hardening (stage I) followed by a much higher but still linear strain-hardening (stage II).

2. In all alloy crystals which exhibited a well-defined, two-stage hardening curve, the extent or amount of shear associated with stage I and the shear-hardening coefficients of stages I and II are significantly dependent on orientation. On approaching the [100], [111] and the [100] – [111] boundary from the [110] (or a decrease in the angle χ_0), the extent of stage I decreases and the shear hardening of both stages I and II increases.

3. For a given alloy composition in the Cu-Al and Cu-Ge systems, the occurrence of a double yield-point is favoured for orientations furthest removed from the [100] – [111] boundary associated with slip on more than one system, or near the [110].

4. For a given solute concentration, the shear stress associated with the onset of stage II is constant and independent of crystal orientation in all alloy crystals examined. Thus, like the onset of stage I with slip on the primary system, the onset of stage II with the occurrence of unpredictable slip on a secondary system appears to be governed by a law of critical resolved shear stress.

4.2. Effect of alloying

1. The critical resolved shear stress for the onset of plastic flow or stage I in the Cu-Al, Cu-Ge and Cu-Si alloy systems increases markedly with increasing solute content but at a decreasing rate. The higher values of this initial flow stress for the Cu-Ge and Cu-Si crystals, as compared to Cu-Al crystals of similar solute concentration, are attributed to their higher concentration of valency electrons.

2. A yield-point phenomenon or double yield-point was observed in Cu-Al and Cu-Ge crystals at high alloy concentrations (> 2 at. %). This yield-point effect becomes more pronounced (upper yield stress minus lower yield stress) with increasing solute content, and eventually replaces the linear hardening of stage I by a yield-point elongation zone of extensive flow at constant stress, or by a region of negative strain-hardening. Strain-anneal experiments strongly suggest that this yield-point effect is due to the anchoring of dislocation lines by Cottrell clouds of solute atoms.

3. The parameters used to characterize the stress-strain diagram are strongly dependent on solid-solution alloying in the three alloy systems examined. For initial orientations which provide a two-stage hardening process, an increase in alloy content results in an increase in the shear associated with the linear hardening of both stages I and II, a decrease in the shear-hardening coefficients of stages I and II, and an increase in the shear stress corresponding to the end of stage II.

4. In all three alloy systems, the critical shear stress associated with the onset of stage II increases markedly with increasing solute concentrations, and at an even more rapid rate than the critical shear stress for the onset of stage I. This is attributed to a more effective pinning with increasing solute concentration of those dislocations responsible for secondary slip on the conjugate or cross-slip systems.

5. The substitution of germanium or silicon for aluminium as a solute in copper results in larger values of shear for stage I, and lower values of shear hardening in stages I and II.

4.3. Slip line observations (Cu-Al alloys)

1. In all alloy crystals examined, the low linear shear hardening in stage I is associated with slip on a single (primary) system, which is distributed uniformly along the entire gauge-length of the crystal.

2. The decrease in the shear-hardening of stage I with increasing solute concentration is attributed to an accompanying increase in the

tendency for slip lines to cluster into bands with increasing elongation.

3. In crystals with high solute concentrations and with stress-strain diagrams exhibiting a yield-point phenomenon, primary slip band development in stage I still remains uniform along the length of the crystal.

4. The onset of stage II is accompanied by unpredicted secondary slip on the conjugate and/or cross-slip systems, and the ensuing high linear shear-hardening is related to the pattern of intersecting slip markings associated with this multiple glide.

5. The decrease in the shear-hardening coefficient of stage II with increasing solute concentration is attributed to a corresponding decrease with increasing deformation in the number of intersecting slip lines resulting from the preferential occurrence of secondary slip between bands of primary slip, and the increased tendency for secondary slip lines to cluster into bands.

6. The high linear shear-hardening associated with critical orientations near the [100] – [111] symmetry position is due to a uniform pattern of intersecting slip lines on the primary and conjugate planes; no evidence of cross-slip or clustering of slip lines were observed.

7. The high linear shear-hardening associated with the critical orientation near the [111] is due to simultaneous slip on the primary, conjugate and cross-slip systems; with increasing solute concentration clustering of slip lines into large bands occurs predominantly on the primary and cross-slip systems, resulting in a highly heterogeneous pattern of slip band development on these systems.

8. The higher degree of shear-hardening for the [111] orientation as compared to the [100] – [111] for similar solute concentrations is attributed to the greater multiplicity of glide accompany slip on three systems as against two.

9. No evidence of kink band formation or twinning was observed for extensions up to 16% and solute concentrations as high as 8%.

Acknowledgement

The author wishes to express his gratitude to Mr J. F. Black, General Telephone and Electronic Laboratories, for his skilful assistance in carrying out various aspects of the experimental programme, and to Dr M. S. Abrahams of RCA Laboratories for assistance in compiling the data.

References

1. J. O. LINDE, B. O. LINDELL, and C. H. STADE, *Ark. Fys.* **2** (1950) 89; **8** (1954) 511.
2. G. W. ARDLEY and A. H. COTTRELL, *Proc. Roy. Soc. A* **219** (1953) 328.
3. G. R. PIERCY, R. W. CAHN, and A. H. COTTRELL, *Acta Metallurgica* **3** (1955) 331.
4. B. JAOUL, *C.R. Acad. Sci., Paris* **240** (1955) 2532.
5. J. GARSTONE, R. W. K. HONEYCOMBE, and G. GREETHAM, *Acta Metallurgica* **4** (1956) 485.
6. R. E. JAMISON and F. A. SHERILL, *ibid* **4** (1956) 197.
7. J. GARSTONE and R. W. K. HONEYCOMBE, "Dislocations and Mechanical Properties of Crystals" (Wiley, New York, 1957) p. 391.
8. H. SUZUKI, S. SKEDA, and S. TAKEUCHI, *ibid* p. 361.
9. K. SCHRÖDER, *Proc. Phys. Soc. Lond.* **72** (1958) 33; **73** (1959) 674.
10. J. MEISSNER, *Z. Metallk.* **50** (1959) 207.
11. P. HAASEN and A. KING, *ibid* **51** (1960) 722.
12. T. J. KOPPENAAL and M. E. FINE, *Trans. AIME* **221** (1961) 1178; **224** (1962) 347.
13. A. A. HENDRICKSON and M. E. FINE, *ibid* **221** (1961) 103; **221** (1961) 967.
14. S. MADER, "Electron Microscopy and the Strength of Crystals" (Interscience, New York, 1963) p. 183.
15. T. E. MITCHELL and P. R. THORNTON, *Phil. Mag.* **8** (1963) 1127.
16. C. F. ELAM, *Proc. Roy. Soc.* **115** (1927) 133.
17. *Idem, ibid* **115** (1927) 148.
18. *Idem, ibid* **116** (1927) 694.
19. R. KARNOP and G. SACHS **49** (1928) 480.
20. M. MASIMA and G. SACHS, *Z. Physik* **50** (1928) 161.
21. V. GÖLER and G. SACHS, *ibid* **55** (1929) 581.
22. G. SACHS and J. WEERTS, *ibid* **62** (1930) 473.
23. *Idem, ibid* **67** (1931) 507.
24. E. OSSWALD, *ibid* **83** (1933) 55.
25. L. M. CLAREBROUGH and M. E. HARGREAVES, *Prog. Met. Phys.* **8** (1959) 1.
26. T. E. MITCHELL, *Prog. Appl. Mat. Res.* (1967) 119.
27. R. G. TREUTING and R. M. BRICK, *Trans. AIME* **147** (1942) 128.
28. R. MADDIN, C. H. MATHEWSON, and W. R. HIBBARD, *ibid* **175** (1948) 86.
29. D. KUHLMANN-WILSDORF and H. WILSDORF, *Acta Metallurgica* **1** (1953) 394.
30. H. WILSDORF and J. T. FOURIE, *ibid* **4** (1956) 271.
31. G. MASING and J. RAFFELSIEPER, *Z. Metallk.* **41** (1950) 65.
32. K. LÜCKE and H. LANGE, *ibid* **43** (1952) 55; **44** (1953) 183 and 514.
33. F. D. ROSI, *Trans. AIME* **200** (1954) 1009.
34. H. SUZUKI, S. IKEDA, and S. TAKEUCHI, *J. Phys. Japan* **11** (1956) 382.
35. J. GARSTONE, R. W. K. HONEYCOMBE, and G. GREETHAM, *Acta Metallurgica* **4** (1956) 585.
36. W. SCHÜLE, O. BUCK, and W. KÖSTER, *Z. Metallk.* **53** (1962) 172.
37. E. N. DA C. ANDRADE and C. HENDERSON, *Phil.*

Trans. **244** (1951) 177.
38. L. PAULING, "The Nature of the Chemical Bond" (Cornell University Press, Ithaca, New York, 1945) p. 64 and p. 346.
39. P. W. BRIDGMAN, *Proc. Amer. Acad. Arts and Sci.* **58** (1923) 165; **60** (1925) 305.
40. M. J. BUERGER, *Z. Krist.* **89** (1934) 193.
41. F. D. ROSI, *Rev. Sci. Instr.* **22** (1951) 708.
42. E. SCHMID and W. BOAS, "Kristallplastizität" (Springer, Berlin, 1935).
43. F. D. ROSI and C. H. MATHEWSON, *Trans. AIME* **188** (1950) 1159.
44. J. DIEHL, *Z. Metallk.* **47** (1956) 331; **47** (1956) 441.
45. M. S. PATERSON, *Acta Metallurgica* **3** (1955) 491.
46. R. F. MILLER and W. E. MILLIGAN, *Trans. AIME* **124** (1937) 229.
47. R. KARNOP and G. SACHS, *Z. Angew. Physik* **41** (1927) 116.
48. G. I. TAYLOR, *Proc. Roy. Soc.* **116** (1927) 39.
49. W. BOAS and E. SCHMID, *Z. Angew. Physik* **71** (1931) 703.
50. A. H. COTTRELL, "The Strength of Solids" (Physical Society, London, 1948) p. 30.
51. *Idem*, "Plastic Deformation of Crystalline Solids" (Mellon Institute, Pittsburgh, 1950) p. 60.
52. W. M. LOMER, *Phil. Mag.* **42** (1951) 1327.
53. A. H. COTTRELL, *ibid* **43** (1952) 645.

Received 3 July 1972 and accepted 20 January 1973.